

Low temperature terahertz spectroscopy of n -InSb through a magnetic field driven metal-insulator transition

X. P. A. Gao, J. Y. Sohn, and S. A. Crooker

National High Magnetic Field Laboratory, Los Alamos, NM 87545

(Dated: February 20, 2022)

We use fiber-coupled photoconductive emitters and detectors to perform terahertz (THz) spectroscopy of lightly-doped n -InSb directly in the cryogenic (1.5 K) bore of a high-field superconducting magnet. We measure transmission spectra from 0.1-1.1 THz as the sample is driven through a metal-insulator transition (MIT) by applied magnetic field. In the low-field metallic state, the data directly reveal the plasma edge and magneto-plasmon modes. With increasing field, a surprisingly broad band (0.3-0.8 THz) of low transmission appears at the onset of the MIT. This band subsequently collapses and evolves into the sharp $1s \rightarrow 2p^-$ transition of electrons ‘frozen’ onto isolated donors in the insulating state.

PACS numbers: 71.30.+h, 78.47.+p, 71.55.-i, 78.20.Ls

Metal-to-insulator transitions (MITs) in condensed matter have fascinated researchers for decades [1]. MITs have been studied as a function of doping, disorder, pressure and magnetic field (B), and two general pictures have emerged [2]. The first concerns Anderson’s notion of disorder-induced localization [3]. Alternatively, Mott’s picture relates the MIT to the overlap between electron wavefunctions in a uniform ionic lattice. The inevitable presence of disorder in real samples usually entangles these two mechanisms, and their effects are hard to separate. Owing to its continuous tunability, the B -induced MITs in lightly-doped semiconductors (*e.g.* InSb, HgCdTe, GaAs) are of particular interest, for which many mechanisms have been proposed including magnetic freezeout, Anderson localization, a Mott transition, and even Wigner crystallization [4, 5, 6, 7]. The more recent observation of an impurity-shifted cyclotron resonance on the *metallic* side of this MIT in n -HgCdTe and n -InSb suggests that B freezes mobile electrons onto donor impurities within a metallic impurity band [5, 6, 7].

Complementing traditional dc transport methods, high frequency spectroscopy of MITs elucidate the *dynamics* and *excitations* involved. For example, the doping-tuned MIT in NbSi alloys reveals ω/T scaling in the ac conductivity from 0.1-1 THz [8], which points to the quantum-critical nature of this MIT. For the low-density metals realized in lightly-doped semiconductors, all the relevant frequency (energy) scales generally lie in the THz (meV) range. Consider Te-doped n -InSb, with $n = 5 \times 10^{14}/\text{cm}^3$: The Fermi energy is 1.6 meV (0.39 THz) and the plasma frequency $\omega_p = (ne^2/\epsilon\epsilon_0 m^*)^{1/2} = 2\pi \times 0.42$ THz ($\epsilon \approx 16$ and $m^* = 0.014 m_e$). The Te donor binding energy is ~ 2 meV at 1 T [9], the cyclotron frequency $\omega_c = eB/m^* \equiv 2\pi \times 2$ THz/T, and a MIT is induced at a critical magnetic field $B_{MIT} \sim 1$ T [7]. It is clearly desirable, therefore, to probe this B -induced MIT using broadband THz spectroscopy spanning these relevant

cavity methods and far-infrared (FIR) optical spectroscopies, standard time-domain THz methods (using free-space lasers, micropositioning stages, and large THz optics) are not generally suited to the narrow and physically remote low-temperature bores of high-field solenoids. We therefore developed miniature fiber-coupled emitters and detectors for time-domain THz spectroscopy directly in the cryogenic bores of superconducting magnets [10].

Using these recently-developed techniques, we report on the THz transmission spectra through a series of lightly Te-doped bulk n -InSb samples as they are field-tuned through B_{MIT} ($n = 2\text{--}11 \times 10^{14}/\text{cm}^3$). At low B , we directly observe the plasma edge and coupled magneto-plasmon modes of the low-density metal. Most strikingly, as B is tuned through B_{MIT} , we observe an abrupt drop in the THz transmission over a surprisingly broad frequency band (0.3-0.8 THz), which rapidly narrows and evolves into the sharp $1s \rightarrow 2p^-$ transition (at ~ 0.3 THz) characteristic of electrons ‘frozen’ onto Te donors in the insulating state. These spectroscopic terahertz data therefore provide detailed insight into low-energy electron dynamics through a continuously-tunable MIT.

The experiment (Fig. 1a) is essentially time-domain THz spectroscopy using photoconductive antennas [11], but with the THz emitter and detector antennas located directly in the 1.5-300 K insert of a high-field, 17 T superconducting solenoid magnet. The antennas are fiber-coupled, and ultrafast optical pulses from a Ti:Sapphire laser (800 nm) are used to drive the emitter and gate the detector. Material dispersion in the fibers requires pre-chirping (stretching) the ultrafast pulses so that they arrive at the antennas, after 20m of fiber, with ≤ 200 fs pulsewidth (see Ref. [10] for details). The samples are mounted between the THz emitter and detector, on a rotating stage that moves the sample in and out of the THz beam path (for background spectra at each B , T).

Figure 1b shows the normalized THz transmission spectra through a 0.8 mm thick sample of n -InSb with $n = 2.1 \times 10^{14}/\text{cm}^3$, at 1.7 K. Power spectra are recorded

While bridging the frequency gap between microwave

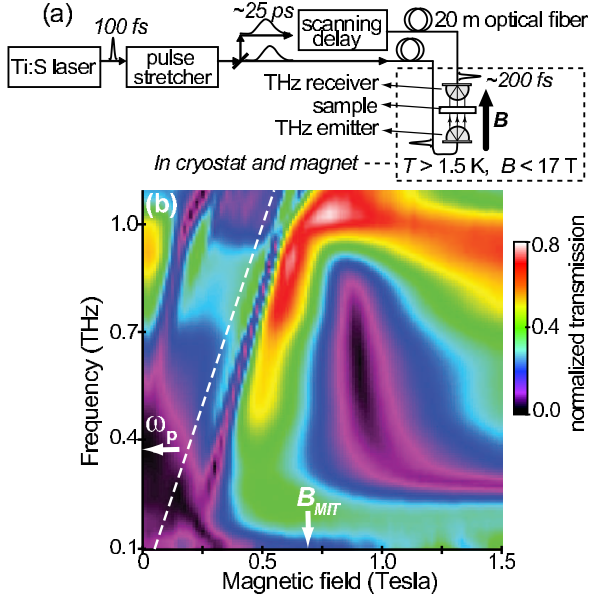


FIG. 1: (Color online) (a) THz spectroscopy with fiber-coupled antennas. (b) THz transmission spectra through bulk (0.8 mm thick) Te-doped n -InSb vs. B at 1.7 K ($n=2.1 \times 10^{14}/\text{cm}^3$). Black regions indicate low transmission, from strong absorption or reflection by the sample. Dotted line represents the one-electron cyclotron frequency, eB/m^* .

vertically, with frequency increasing from 0.1 to 1.1 THz along the y-axis. B increases from 0 to 1.5 T along the x-axis. Zero (or low) transmission is represented by a black color, implying strong absorption or reflection of the THz radiation by the sample. We focus primarily on these black regions, which indicate the presence of cyclotron resonance (CR), impurity transitions, or magneto-plasma reflectivity edges. For reference, the CR frequency within a one-electron model (2 THz/T) is plotted as a dashed white line. At $B=0$ the sample is metallic, and careful inspection reveals no transmission below 0.38 THz, indicating the total reflection of light below the plasma frequency ω_p of this low-density metal. In small B , the cyclotron motion of free electrons couples to plasma oscillations and the plasma edge splits into two magneto-plasmon modes [13]: $\omega_{\pm} = [(4\omega_p^2 + \omega_c^2)^{1/2} \pm \omega_c]/2$. These modes are directly observed in the spectroscopic data. The ω_- branch is revealed by the border of the low transmission region at the bottom left, and the ω_+ branch is observed as the dark line with positive slope originating at ω_p . Lastly, a transition line with slope close to the CR (but shifted to higher B) appears for $B \gtrsim 0.25$ T (to be discussed). These low-field THz data therefore directly reveal how a free-electron metal evolves into a system of coupled magnetoplasmon modes.

The most striking feature in Fig. 1b, however, is the sudden onset at $B \sim 0.8$ T of low THz transmission over a wide frequency band from 0.3-0.8 THz. This region narrows quickly with increasing B , collapsing towards the

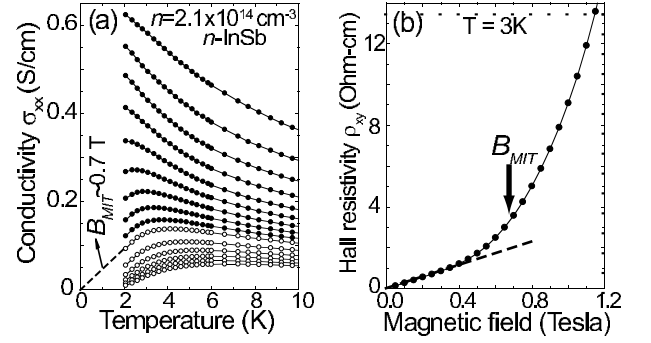


FIG. 2: (a) The dc conductivity σ_{xx} vs. T of n -InSb at $B = .25, .3, .35, .4, .45, .5, .55, .6, .65, .7, .8, .9, 1.0, 1.1$ and 1.2 T (top to bottom). $B_{MIT} \sim 0.7$ T, as given by the field where σ_{xx} extrapolates linearly to zero as $T \rightarrow 0$ (dotted line). (b) The Hall resistivity ρ_{xy} vs. B at $T=3$ K. Near B_{MIT} , ρ_{xy} begins diverging, indicating electron freeze-out.

known $1s \rightarrow 2p^-$ transition energy (~ 0.3 THz) of electrons bound to Te donors [9, 14]. We associate this marked feature with the onset of the field-induced MIT, and indeed we confirm that $B_{MIT} = 0.7$ T in this sample by conventional dc transport. Fig. 2a shows the temperature-dependent dc conductivity $\sigma_{xx}(T)$ from $B = 0.2$ -1.2 T (the 2 K electron mobility $\mu = 7.7 \times 10^4 \text{ cm}^2/\text{Vs}$, suggesting a mean scattering time $\tau = 0.6$ ps). In the low-field metallic state σ_{xx} tends to finite values as $T \rightarrow 0$, while in the high-field insulating state $\sigma_{xx} \rightarrow 0$ as $T \rightarrow 0$. As conventionally defined by the field at which σ_{xx} extrapolates linearly to zero as $T \rightarrow 0$ [6, 7], we find that $B_{MIT} = 0.7$ T, in agreement with previous transport studies of similarly-doped n -InSb. Also in agreement with prior work [6], the Hall resistivity ρ_{xy} , which is inversely proportional to the free electron density, begins to diverge near B_{MIT} (see Fig. 2b). These transport data are characteristic of the MIT in n -InSb induced by magnetic freeze-out of the mobile electrons.

The abrupt disappearance of transmitted radiation from 300-800 GHz therefore occurs at magnetic fields just above the value of B_{MIT} that is conventionally defined by dc transport. The THz data suggest this phenomenon may be generic – similar behavior is observed in *all* the n -InSb samples ($n = 2.1, 3.4, 5, 6$, and $11 \times 10^{14}/\text{cm}^3$). Fig. 3a shows THz transmission through the higher-doped $n = 6 \times 10^{14}/\text{cm}^3$ sample at 1.5 K. Again, a broad region of low transmission appears just above B_{MIT} ($= 1.1$ T at this higher density). This region again narrows as $B > B_{MIT}$, evolving continuously into the sharp $1s \rightarrow 2p^-$ donor transition at ~ 0.3 THz [9, 14, 15]. As expected for a $1s \rightarrow 2p^-$ transition [9], we confirm that this absorption shifts to slightly higher energy (0.4 THz) as $B \rightarrow 15$ T, and disappears for $T > 10$ K (due to thermal ionization of donor-bound electrons).

Importantly, *no sign* of a $1s \rightarrow 2p^-$ donor transition is observed in the THz spectra at low B when the sample is

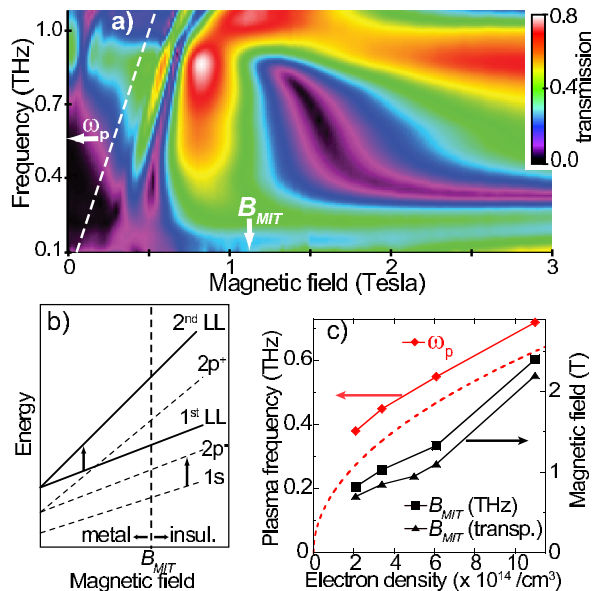


FIG. 3: (Color online) (a) THz transmission through n -InSb vs. B at 1.5 K ($n = 6 \times 10^{14}/\text{cm}^3$). (b) Schematic of the 1st and 2nd Landau levels (solid) and the $1s$, $2p^+$, $2p^-$ donor levels (dashed) vs. B . Arrows mark the relevant transitions. (c) Doping dependence of the measured plasma edge (red diamonds; dashed line is the calculated ω_p), and of B_{MIT} as measured by transport (triangles) and THz data (squares).

in the metallic state. Careful FIR magneto-transmission studies at single frequencies (0.75-2 THz) have suggested that the MIT in n -InSb occurs within a metallic impurity band [6]. These new spectroscopic THz measurements suggest that near B_{MIT} , the impurity band may broaden significantly, allowing excitations over a wide range of frequencies. These data are reminiscent of the doping-tuned MIT in phosphorous-doped Si, where sharp transitions from donor-bound electrons were observed deep in the insulating (low-doped) state [12]. These transitions broadened as doping increased toward the critical density, due to donor-donor interactions and the formation of donor clusters. A similar picture can be applied to the present case of n -InSb. In the insulating state ($B \gg B_{MIT}$), electrons are “frozen” onto individual donors and sharp $1s \rightarrow 2p^-$ transitions from effectively isolated donors are seen. As B decreases towards B_{MIT} , the Bohr radii of bound electrons grows, interactions and wavefunction overlap become significant, and the notion of a discrete impurity transition becomes ill-defined. This scenario is consistent with the spirit of a Mott transition.

Within a simplified one-electron framework, Fig. 3b sketches the relevant free-electron Landau levels (LL) and donor-bound electron states in n -InSb. The $1s$ and $2p^-$ donor states follow the 1st LL [9, 13, 15]. Dominant transitions are marked by arrows: i) the (plasmon-shifted) inter-LL CR of free electrons, and ii) the $1s \rightarrow 2p^-$ transition of

electrons frozen onto donors in the insulating state (the $1s \rightarrow 2p^0$ is forbidden in the Faraday geometry [15]). As a function of electron density, Fig. 3c summarizes the key parameters from the THz magneto-transmission experiments. First, diamonds represent the $B=0$ plasma edge, as measured by the point below which no transmission is observed. These values agree reasonably well with a calculation of $\omega_p/2\pi$ (dashed line). Secondly, the field at which THz transmission becomes abruptly suppressed (squares) is shown to track B_{MIT} as determined from dc transport (triangles), suggesting their common origin and a possible broadening of an impurity band at B_{MIT} . Note that we cannot distinguish the $1s \rightarrow 2p^+$ impurity CR [6, 9, 14, 15] from the nearby plasma-shifted CR in our experiment. Further studies may clarify the nature of the additional transition observed in both Figs. 1b and 3a (having slope $\sim eB/m^*$, but shifted to higher B /lower energy). Although expected to be weak, a possible transition in these thick samples from the 1st LL $\rightarrow 2p^+$ is consistent with the observed slope and shift of this line.

These data lend insight into the high-frequency dynamics of electrons undergoing a metal-insulator transition, and highlight the utility of *in situ* low-temperature broadband THz spectroscopy in magnetic fields using fiber-coupled antennas. Transmission of THz photons through n -InSb directly reveals the splitting of the plasma edge into magnetoplasmon modes in the metallic state ($B < B_{MIT}$). In contrast, data in the high-field insulating state ($B \gg B_{MIT}$) directly reveal the sharp $1s \rightarrow 2p^-$ transition of electrons “frozen” onto donor impurities. As B decreases toward B_{MIT} , the sharp $1s \rightarrow 2p^-$ transition widens into a broad band with low THz transmission, suggesting the broadening of an impurity band at B_{MIT} . We thank D. L. Smith, G. S. Boebinger, P. B. Littlewood, B. McCombe, J. Kono, and S. Kos for valuable discussions, and the NHMFL IHRP and Los Alamos LDRD programs for support.

-
- [1] N. F. Mott, *Metal-Insulator Transitions* (Taylor and Francis, London, 1990).
 - [2] D. Belitz and T. R. Kirkpatrick, Rev. Mod. Phys. **66**, 261 (1994).
 - [3] P. W. Anderson, Physical Review **109**, 1492 (1958).
 - [4] R.W. Keyes and R. J. Sladek, J. Phys. Chem. Solids, **1**, 143 (1956).
 - [5] V. J. Goldman, H. D. Drew, M. Shayegan and D. A. Nelson, Phys. Rev. Lett. **56**, 968 (1986).
 - [6] M. Shayegan, V. J. Goldman and H.D. Drew, Phys. Rev. B **38**, 5585 (1988); J. B. Choi, S. Liu and H. D. Drew, Phys. Rev. B **43**, 4046 (1991).
 - [7] R. G. Mani, L. Ghenim and J. B. Choi, Phys. Rev. B **43**, 12630 (1991).
 - [8] H.-L. Lee *et al.*, Science **287**, 633 (2000).
 - [9] R. Kaplan, Phys. Rev. **181**, 1154 (1969); R. Kaplan, R. A. Cooke, R. A. Stradling, Solid State Comm. **26**, 741

- (1978); W. Zawadski, in *Landau Level Spectroscopy*, G. Landwehr, E. I. Rashba, Eds (North-Holland, Amsterdam, 1991).
- [10] S. A. Crooker, Rev. Sci. Instrum. **73**, 3258 (2002).
 - [11] N. Katzenellenbogen and D. Grischkowsky, Appl. Phys. Lett. **58**, 222 (1993).
 - [12] G. A. Thomas *et al.*, Phys. Rev. B **23**, 5472 (1981).
 - [13] E.D. Palik, G.S. Picus, S. Teitler and R. F. Wallis, Phys. Rev. **122**, 475 (1961); E.D. Palik and J.K. Furdyna, Rep. Prog. Phys. **33**, 1193 (1970).
 - [14] Y. Yafet, R. W. Keyes, and E. N. Adams, J. Phys. Chem. Solids **1** 137 (1956); D. M. Larsen, J. Phys. Chem. Solids **29**, 271 (1968).
 - [15] B. D. McCombe and R. J. Wagner, Adv. Electronics and Electron Phys. **38**, 1-53 (1975).